THE AMERICAN SOCIETY OF MECHANICAL ENGINEERS
345 E. 47th St., New York, N.Y. 10017

96-GT-359

THE EFFECT OF VORTEX SHEDDING ON THE UNSTEADY PRESSURE DISTRIBUTION AROUND THE TRAILING EDGE OF A TURBINE BLADE

G. Cicatelli C.H. Sieverding
von Karman Institute - Belgium

ABSTRACT

The wakes behind turbine blade trailing edge are characterized by large scale periodic vortex patterns known as the von Karman vortex street. The failure of steady-state Navier-Stokes calculations in modeling wake flows appears to be mainly due to ignoring this type of flow instabilities. In an effort to contribute to a better understanding of the time varying wake flow characteristics behind turbine blades, VKI has performed large scale turbine cascade tests to obtain very detailed information about the steady and unsteady pressure distribution around the trailing edge of a nozzle guide vane. Tests are run at an outlet Mach number of $M_{2is}=0.4$ and a Reynolds number of $Re_C = 2 \cdot 10^6$. The key to the high spatial resolution of the pressure distribution around the trailing edge is a rotatable trailing edge with an embedded miniature pressure transducer underneath the surface and a pressure slot opening of about 1.5° of the trailing edge circle. Signal processing allowed or differentiation between random and periodic pressure fluctuations. Ultra-short schlieren pictures help in understanding the physics behind the pressure distribution.

NOMENCLATURE

C	Turbine blade mechanical chord
C_{ax}	Axial chord
C_{Pb}	Base pressure coefficient
D	Turbine blade trailing edge thickness
g	Pitch
h	Blade height
M_{2is}	Isentropic outlet Mach number
o	Throat opening
P_b	Base pressure
P_{01}	Inlet total pressure
P_{S2}	Outlet static pressure
Re_C	Reynolds number based on chord length
S	Curvilinear abscissa
T_{01}	Inlet total temperature
Tu	Inlet turbulence level
u	Boundary layer velocity
u_e	Boundary layer external velocity
W_{max}	Blade velocity peak
W_2	Blade outlet velocity
X	Axial direction

Greek symbols

α_2^*	Gauging angle (arcsin o/g)
α	Probe angle
γ	Stagger angle
δ	Boundary layer thickness
δ^*	Boundary layer displacement thickness
ε	Wedge angle
θ	Boundary layer momentum thickness
ρ	Air density
ω	Total pressure loss coefficient

1. INTRODUCTION

The steady state approach for solving turbomachinery flow problems which has prevailed for many decades of turbomachinery research is progressively being abandoned in favor of the study of the true unsteady character of the flow through the bladings. The recent rapid increase of experimental and numerical research project devoted to the wake-blade interaction phenomena in stages clearly demonstrates this new view point. The intensity of the periodic phenomenon, which is related to the blade passing frequency, directly depends on the pressure gradient field generated by the wake at the inlet to the downstream blade row and thereby on the mixing process of the wake.

Presented at the International Gas Turbine and Aeroengine Congress & Exhibition
Birmingham, UK — June 10-13, 1996
This paper has been accepted for publication in the Transactions of the ASME
Discussion of it will be accepted at ASME Headquarters until September 30, 1996

To date, the mixing process of the wake behind a turbine (or compressor) blade is still viewed as a steady state process, although it is well known that the separation of the boundary layers at the trailing edge is an highly unsteady phenomenon which leads to the formation of large coherent structures, known as the von Karman vortex street. For turbine blades the vortex shedding frequency is typically between 5 and 50 kHz.

Steady state Navier-Stokes calculations using conventional mixing length and 2-equations models, fail to correctly predict the wake evolution behind turbomachinery blading for two reasons: (a) they ignore the strong time varying character of the wake flow and (b) they are unable to deal with the highly non-isotropic character of turbulent separated flows and wake flows. Unsteady Navier-Stokes solvers, improved turbulence models like non linear 2-equations and Reynolds stress models and Large-Eddy Simulation techniques are presently investigated regarding their suitability for the calculation of the wake mixing process.

The technical literature concerning the investigation of unsteady turbine wake characteristics is rather scarce, see Cicatelli and Sieverding [1]. To-date the most comprehensive studies are those by Lawaczeck and Heinemann [2] on the effect of boundary layer state on vortex shedding from flat plates and turbine cascades, on vortex shedding frequency measurements for a wide variety of cascades by Sieverding and Heinemann [3], and on the observation of different types of vortex streets behind turbine blades by Carscallen and Gostelow [4]. None of these studies reported any detailed quantitative measurements on the time varying trailing edge flow and wake flow characteristics. The reason for this is the relative small trailing edge size of most cascade blades which does not allow for a sufficient spatial resolution for detailed investigations in the most important region, i.e. the near-wake flow region. Clearly only large scale models can provide sufficient spatial resolution for detailed flow field measurements.

Large scale models were already used by Han and Cox [5] for Smoke visualizations of the von Karman vortex street in the wake of a low speed nozzle guide vane and by Mee [6] for detailed measurements of boundary layer characteristics and pressure distribution in the trailing region. Our present knowledge on the mechanism of vortex formation, turbulence production and dissipation however is entirely based on research of the flow over large scale bluff bodies, e.g. [7] [8] [9]. But these results can not be transferred directly to turbine blades because of the different flow conditions for flows separating from bluff bodies and from turbine blades: blade circulation and different boundary layers states on pressure and suction side before separation for turbine blades, symmetric flow conditions for bluff bodies.

The investigations reported in this paper are part of a BRITE EURAM project. The aim of the project is twofold: (a) to improve our understanding of physics of unsteady turbine blade wakes and (b) to provide high quality experimental data for the validation of Navier-Stokes codes. The turbine blade selected for this study is a large scale nozzle guide vane with thick trailing edge. The main scope of this paper is the presentation of detailed measurements of the trailing edge pressure distribution, steady and unsteady. Ultra short schlieren pictures contribute to the interpretation of these data.

2. TUNNEL AND CASCADE MODEL

The tests described in this paper were performed in the VKI high speed cold flow open circuit blow down cascade tunnel.

The overall blade dimensions were determined by the need of the highest possible spatial resolution for the trailing edge pressure, requiring a maximum trailing edge thickness, and the maximum dimensions of the test section i.e. 400 mm heigtht and 200 mm width. The compromise resulted in a 3-bladed cascade with blades of 280 mm chord length, 200 mm blade height and 15 mm trailing edge thickness, Fig. 1.

The blade was designed front loaded with an overall low suction side turning in the overhang section and in particular a straight rear suction side from half way down the throat. These design features met the following requirements:

a) to ensure a turbulent state of the suction side boundary layer at the trailing edge

b) to easy the use of tailboards (easier with a weakly curved rear suction side than with a highly curved rear suction side)

c) to easy the implementation of an optical window in the rear suction side of the lower blade of the cascade for PIV measurements in a later phase of the project.

The fine tuning of the blade shape was accomplished using a semi-inverse blade design method by Leonard and van den Braembussche [10]. The most important geometrical dimensions of the cascade are summarized below:

chord length C	=	280 mm
pitch to chord ratio g/C	=	0.696
blade height h	=	200 mm
aspect ratio h/C	=	0.7
trailing edge to chord ratio D/C	=	0.0531
trailing edge wedge angle ε	=	7.5°
stagger angle γ	=	-49°83
gauging angle α_2^* (arcsin o/g)	=	19.1°

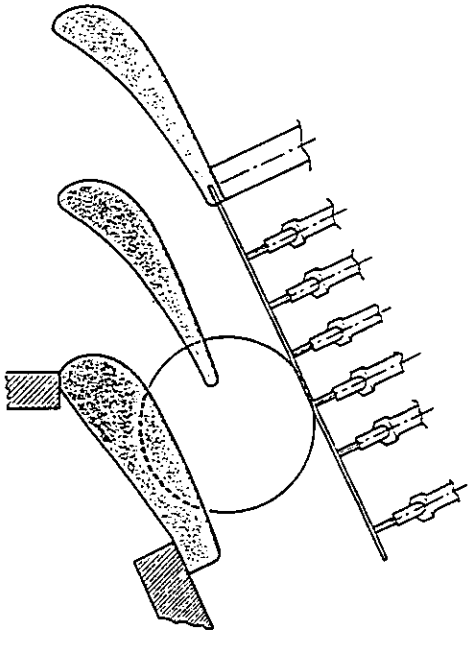

Fig. 1: Blade model and cascade test section

The blade coordinates are given in the annexe.

2. BLADE INSTRUMENTATION

A first blade (Blade A) was equipped with 31 wall pressure tappings along the suction side and 22 tappings along the pressure side at mid span to determine the blade velocity distribution. Regarding the trailing edge, the placement of individual pressure tappings around the trailing edge would not have provided the required dense spatial distribution in this region. Therefore, the blade trailing edge is designed with a rotatable cylinder of 20 mm height placed at mid span, Fig.2-a. This cylinder is equipped with a single Kulite pressure sensor and an ordinary pneumatic pressure tapping implemented side by side.

The need of a high frequency response ideally requires the transducer to be surface mounted. The relative large diameter of the Kulite transducer (type XCS-062 5PSI) poses a severe limitation to the spatial resolution. A 1.62 mm diameter surface mounted transducer on a 15 mm diameter circular trailing edge covers an angular sector of 12.4°.

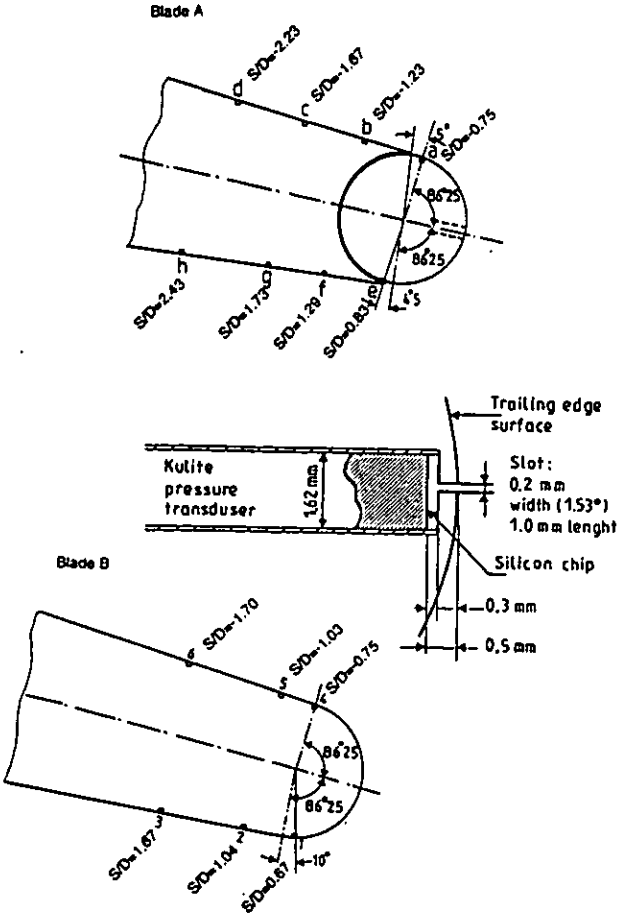

Fig.2-a,b,c: Blades instrumentation

To reduce the opening angle, the transducer is mounted underneath the trailing edge surface and connected to the external environment via a small rectangular window of 1.0 mm length and 0.2 mm width, reducing the sensing area to an angular sector of 1.53° only. Notice that the area of this window is equal to the total area of the opening in a typical "B" screen frequently mounted by the manufacturer on these transducers. The total distance between the trailing edge surface and the transducer chip is 0.5 mm: a depth of the rectangular slot of 0.3 mm and a retreat of the pressure chip from the head of the Kulite probe of 0.2 mm, Fig.2-b. The opening of the pneumatic pressure tapping is the same as for the Kulite i.e. 1x0.2 mm. The rotatable cylinder is rigidly connected to a manual device enabling the rotation of the cylinder. The angular position is controlled with a circular protractor. With a gap of ~0.01 mm between the rotatable cylinder and the blade and a thickness of the blade lips of ~0.02 mm, the angular position of the lips with respect to the tangential points of the ideal blade surfaces to the trailing edge circle are 5° and 4.5° for the suction side and pressure side respectively, Fig.2-a.

A second blade (Blade B) was instrumented with six Kulite transducers placed at and slightly upstream of the trailing edge, Fig.2-c. The manufacturing of this second blade was suggested by the need to verify the possible influence of the rearward facing step between the blade lip and the rntatable cylinder on blade A and to obtain information on the effects of the vortex shedding on the flow upstream of the trailing edge. Each Kulite transducer is coupled with a pressure tap following the same criteria used for blade A. The exact positions are indicated in Fig.2-c. The Kulite transducer Nr.1 is placed on the pressure side of the trailing edge surface, 10° from the tangent point, while Nr.4 is placed on the suction side exactly on the tangent point. The transducers 2,3,5,6 are located on the pressure side and suction side respectively at 1.5% and 5% of the mechanical chord from the tangent points.

The frame of reference in which all data will be represented is illustrated on Fig.3. The origin of the reference system is fixed on the centre of the trailing edge. All the data are presented in curvilinear abscissa non-dimensionalized by the trailing edge diameter.

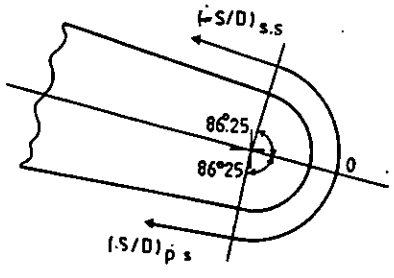

Fig.3: Trailing edge reference system.

3. FLOW CONDITIONS

3.1 Overall conditions

The overall flow conditions for the tests are summarized below:

total pressure upstream P_{01}	=	1178 mbar
total temperature upstream T_{01}	=	287 K
isentropic outlet Mach number $M_{2,is}$	=	0.4
Reynolds number Re_C	=	$2 \cdot 10^6$
degree of turbulence Tu	=	1.15%

3.2 Two dimensionality

In view of the relative small aspect ratio it appeared opportune to attempt to reduce secondary flow effects through the use of boundary layer fences.

Following Kawai [11] the optimum endwall distance of the fences from the side wall is equal to 2/3 of the inlet boundary layer on the side wall. The maximum height of the fence is equal to the blade surface boundary layer thickness close to the trailing edge. Based on inlet endwall boundary layer measurements and blade boundary layer calculations, the fences were placed at 5 mm from the endwall (blade height 200 mm) with a maximum height of 5 mm at the trailing edge.

The effectiveness of the fences was verified by blade surface oil flow visualizations and downstream total pressure probe traverses.

Fig. 4 shows, for the oil flow visualization, the result of the comparison between the lower blade not fenced and the central blade where boundary layer fences were installed. With boundary layer fences two-dimensional conditions exist over approximately 75% of the blade height.

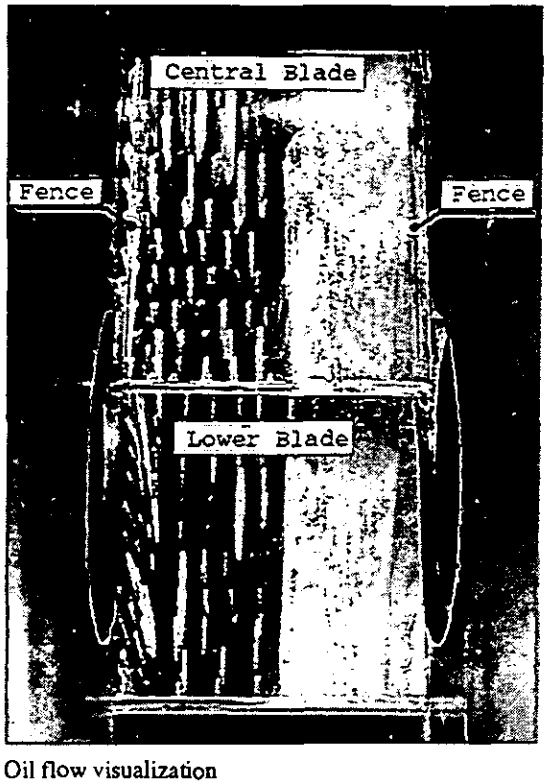

Fig.4: Oil flow visualization

3.3 Periodicity

The use of a flexible tailboard extending from the upper blade allowed to set up a nearly uniform downstream static pressure distribution over both pitches of the cascade, Fig.5

3.4 Blade velocity distribution

The surface pressure distribution is measured using the static pressure tappings on the suction and pressure side of the central blade. The associated mid-span isentropic Mach number distribution is presented in Fig. 6.

The blade velocity is typical for a front loaded blade. The suction side velocity peaks at around $X/C_{ax} \equiv 0.6$ with a ratio of $W_{max}/W_2 = 1.25$. This peak is followed by a smooth deceleration and a plateau on the rear suction side before the start of the trailing edge acceleration. On the pressure side the flow constantly accelerates up to the trailing edge.

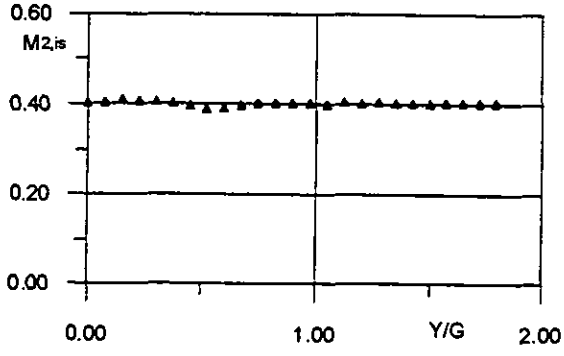

Fig.5: Outlet Mach number disribuion

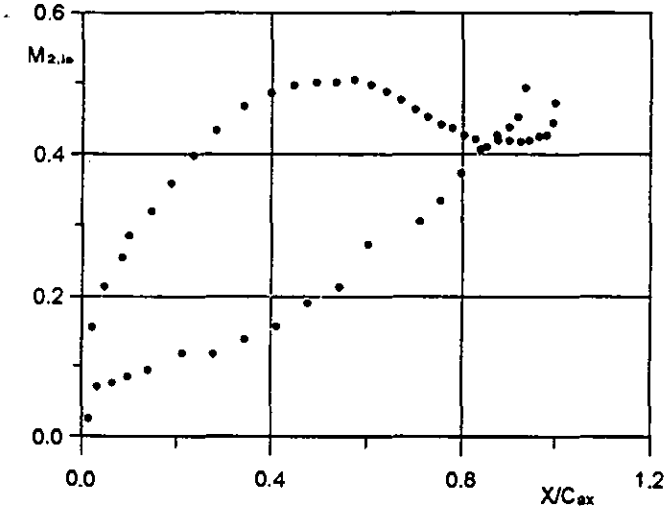

Fig.6: Blade velocity distribution

3.5 Boundary layer characteristics

Sieverding and Heinemann [3] clearly demonstrated that the state of the boundary layer at the trailing edge influences the vortex shedding frequency in the wake. Furthermore the shape of the vortex shedding frequency spectrum depends on the state of the boundary layer on both blade sides. If the boundary layers are laminar or turbulent on both sides, the vortex shedding frequency spectrum is very narrow. In case of mixed laminar/turbulent boundary layers the dominant frequency spectrum tends to broaden. A transitional boundary layer on one or both sides results in a very large vortex shedding frequency spectrum, with possibly the appearance of two maxima. The expected data processing implying conditional phase averaging of the base pressure signal, however requires the identification of a clear peak in the shedding frequency spectrum. The suction side boundary layer is expected to be turbulent at the trailing edge while the pressure side boundary layer is either laminar or transitional. Preliminary tests have led to the decision to trip the boundary layer on the pressure side to have

fullydeveloped turbulent boundary layers on both pressure and suction side. A 0.4 mm diameter trip wire was installed along the span at a station $X / C_{ax} = 0.61$.

Boundary layer profiles were measured with a flattened pitot probe at a distance equal to one trailing edge diameter upstream of the trailing edge circle. The flattened probe had a thickness of 0.25 mm. The uncertainty in the probe position is ±0.05 mm. The characteristics of the compressible boundary layer were determined with the following relationships:

$$\delta^* = \int_0^{\delta} \left(1 - \frac{\rho u}{\rho_e u_e}\right) \cdot dy \qquad (2)$$

$$\vartheta = \int_0^{\delta} \frac{\rho u}{\rho_e u_e} \cdot \left(1 - \frac{u}{u_e}\right) \cdot dy \qquad (3)$$

$$H = \frac{\delta^*}{\vartheta} \qquad (4)$$

Corrections for the displacement effects for pitot tubes in shear flows is of the same order as the uncertainty for the probe position and therefore have been neglected. Correction for the wall interference bave been applied. A second order formula was used:

$$\frac{\Delta u}{u} = \frac{(y/l - 1.9)^2}{1.4^2} \cdot 0.016 \qquad \text{for } y/l < 1.9 \qquad (5)$$

where l is the thickness of the probe head (in this case K=0.25 mm). The boundary layer velocity profiles are presented in Fig.7.

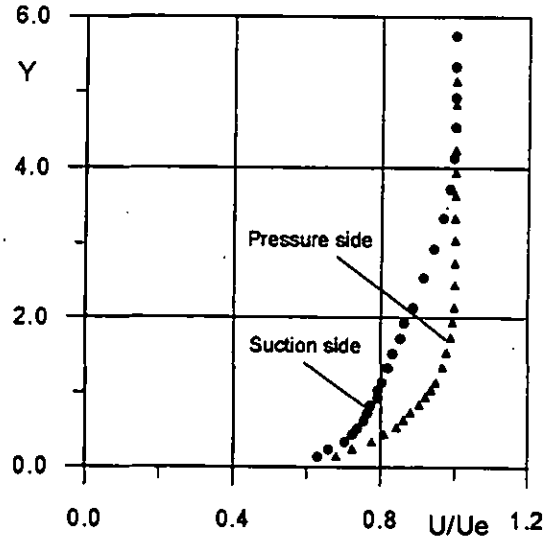

Fig.7: Boundary layer velocity profiles

The boundary layer characteristics are summarized below:

	Pressure Side	Suction Side
δ/D	0.01336	0.2772
δ^*/D	0.0167	0.0405
θ/D	0.0102	0.0288
H	1.64	1.41

The boundary layers are clearly turbulent on both pressure and suction side with the particular characteristic that on the suction side the thickness is approximately the double of that on the pressure side.

4. TRAILING EDGE PRESSURE MEASUREMENTS

4.1 Experimental procedure

The data acquisition was realized with a BE490 acquisition card installed on 486 DX4 100 Mhz PCI bus Personal Computer. The system has a maximum sampling frequency of 1MHz with 12 bits resolution. The board provides access to 8 different channels. The sampling frequency was set to 25 kHz and 4096 samples were acquired. Two channels were dedicated to the acquisition of the trailing edge pressure signal: one for the Kulite pressure transducer and one for the pneumatic static pressure tappings mounted in parallel with the Kulite transducer. In order to guarantee that all the tests were effectively performed at the same outlet flow conditions, for each individual test, the inlet total pressure P_{01} and outlet static pressure P_{S2} were also acquired to determine the outlet Mach number on line.

4.2 Data processing strategy: Signal splitting

In order to analyze the unsteady base pressure, the signal provided by the fast response pressure transducers can be regarded as a combination of a time averaged component $\overline{P}$ and a fluctuating component $\tilde{P}$:

$$P = \overline{P} + \tilde{P} \qquad (6)$$

As regards the time averaged pressure $\overline{P}$, its value can be derived from either the pressure signal of the Kulite transducer or the corresponding pneumatic wall pressure measurements. With a careful adjustement of the zero shift before each blow down of the tunnel the time averaged value of the Kulite transducer signal differed from the pneumatic wall pressure measurements by less than 2%. However the continous adjustement turned out to be a quite tedious task, in particular when recording several transducers simultaneously. It was therefore decided to use the $\overline{P}$ value of the pneumatic wall pressure measurements and use the Kulite signal for the pressure fluctuations only.

A quantitative evaluation of the term $\tilde{P}$ in (6) can be obtained from the root mean square of the fluctuating signal and non-dimensionalized by the dynamic downstream pressure $P_{01} - P_{S2}$:

$$RMS = \frac{\sqrt{\tilde{P}^2}}{P_{01} - P_{s2}} \qquad (7)$$

A further analysis of the term $\tilde{P}$ can be performed starting from the assumption that the term $\tilde{P}$ is the result of two different contributions: a random contribution P' due to the small scale turbulent structures, and a more organized component, essentially periodic, P_{pba}, whose origin can be found in the presence of the organized vortical activity in the wake, mainly the von Karman vortex street:

$$\tilde{P} = P' + P_{pba} \qquad (8)$$

It is not possible to extract directly from the row signal the amplitude of the pressure fluctuation P_{pba}. Then, in order to appreciate the presence of this contribution, a frequency analysis is essential. A Fast Fourier Transform was applied to the fluctuating

part of the pressure signal only, because it was immediately evident that the energy content of the fluctuating part of the signal is much lower than the energy content of the entire signal and this fact could mask the appreciation of the frequency peak in view of a further signal processing.
Once the vortex shedding frequency is identified, it is possible to extract the contribution of the organized vortical activity P_{pha} from the global fluctuating component $\tilde{P}$. For this purpose an ensemble phase averaging technique has been used. The processing is based on the identificatinn of the dominant period T of the signal obtained thanks to the FFT. Then the entire fluctuating signal $\tilde{P}$ is subdivided in pieces of one-period time length T, and eventually a phase averaging of all these small signal is done. This means that every period length signal is further subdivided in a fixed number of intervals. phase averaged over the N cycles of the entire signal. The process can be summarized with the relationship:

$$P_{pha_j} = \frac{1}{N}\sum_j P_{pha_{ij}} \qquad (9)$$

where N is the number of the cycles.

4.3 Vortex shedding frequency

A typical result of the vortex shedding frequency spectrum is shown in Fig.8. This frequency spectrum was measured by a Kulite transducer positioned on the trailing edge circle at α=72° (α=0 correspond to the trailing edge centre) near the point of the highest fluctuations as will be shown later. The dominant frequency peak was found at 2.65 kHz. The frequency is usually expressed by the Strouhal number

$$S = \frac{f \cdot D}{u} \qquad (10)$$

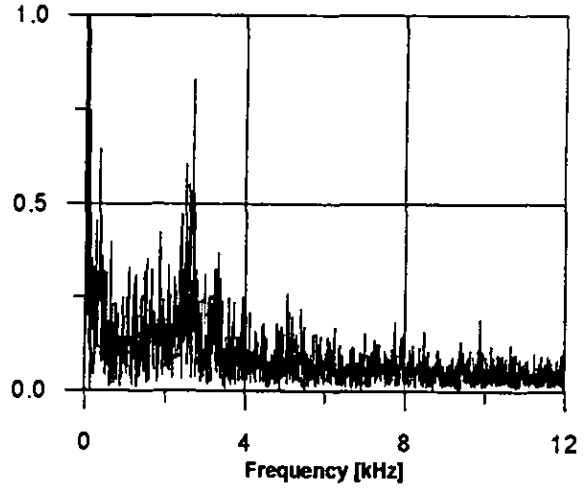

Fig. 8: Vortex shedding frequency spectrum

In cascades the reference velocity "u" is typically taken equal to the downstream velocity. Using this definition the Strouhal number is S=0.27. Comparing the Strouhal numbers from a large number of tests, the authors noticed variation in the Strouhal number of up to 4%, although most tests did not vary by more than 2-3%. These variations are in line with the observation that the dominant frequency does not appear as a single peak in the frequency spectrum but rather as a dominant frequency band width. The Strouhal number of 0.27 is somewhat high for a blade with turbulent boundary layers on both sides of the trailing edge, which appears to be normally in the range S=0.2-0.4 [1]. However, tests at the University of Genova on the same blade with very similar flow conditions showed the same Strouhal number [13].

4.4 Error analysis

The uncertainty related to both instruments mainly depends on the transducer characteristics, on the calibration curve and on the acquisition card characteristics. The acquisition card gives an uncertainty of ± 2.44 mV that corresponds to a card resolution of 1 digit. For the calibration of both transducers, a digital calibrator with an uncertainty of ±0.5 mbar and a voltmeter with an uncertainty estimated around ±5 mV were used. To compute the measurement uncertainty, the following relationship can be used:

$$\delta P = \sqrt{(\delta P_0)^2 + \left(\frac{\partial P}{\partial \alpha}\cdot\delta\alpha\right)^2 + \left(\frac{\partial P}{\partial V}\cdot\delta V\right)^2} \qquad (11)$$

where δP_0 represents the uncertainty related to the zero balance, the second term represents the uncertainty related to the calibration and the last one that related to the acquisition card. For the Validyne transducer used for the pneumatic pressure measurements (steady state measurements) an uncertainty of ±2% of the reference pressure value was found. For the Kulite transducer, the first term is equal to zero because we used only the fluctuating part of the signal. The pressure uncertainty is ±0.17 % of the reference pressure value. Finally the error on the angular positioning of the rotatable cylinder is ±1°.

4.5 Steady state trailing edge pressure distribution

Fig.9 shows the time averaged base pressure distribution around the trailing edge, non-dimensionalized by the inlet total pressure. The frame of reference is the one proposed in Fig.3. The points represented with circles are obtained with the rotatable cylinder while the triangles are obtained from the pressure taps installed on blade A and indicated on Fig.2-b with a-d and e-h. Note that the data designed by a and e are positioned aside the rotatable cylinder at 70 mm from mid-span.
From Fig.8 it results that the flow approaching the trailing edge experiences a strong over expansion compared to the surrounding flow field. Moreover the pressure curve shows a remarkable asymmetry for the pressure side and suction side expansion. The corresponding isentropic peak Mach aumbers together with their exact positions are:

	S/D	α	P_b / P_{01}	Mach
S.S	-0.72	82°5	0.857	0.475
P.S.	0.73	83°6	0.845	0.496

Such high overexpansions could never be reached with a steady state flow separation The peak Mach number exceeds the downstream Mach number by 18.7% and 24% respectively. The higher expansion on the pressure side is probably related to the much thinner boundary layer on the pressure side and to the blade circulation which strengthens the pressure side vortex shedding as suggested by Han and Cox [5]. The pressure distribution shows a

pressure plateau at a value of $P_b / P_{01} \approx 0.885$ extending between the points $S/D = -0.325$ and $S/D = 0.5$. These points correspond to an angle of -37°2 for the suction side and 57°3 on the pressure side, covering globally an angle sector of 94°5. The pressure coefficient describing the pressure in this region, in general referred to as base pressure coefficient, amounts to:

$$C_{Pb} = \frac{P_b - P_{S2}}{P_{01} - P_{S2}} = -0.095 \qquad (12)$$

This value is in good agreement with the base pressure coefficient derived from the correlation by Sieverding et al. [12]. It is interesting to notice that on the pressure side of the base pressure region, around S/D=0.5, the graph shows a significant dispersion of the pressure data which is not observed on the suction side. The enlargment of the region shows however, instead of a random scatter, an ordered fluctuating pressure distribution which is maximum in the transition from the base pressure plateau to the rapid pressure drop and is gradually damped out towards the centre of tbe plateau pressure. An explanation for this phenomenon cannot be given at present.

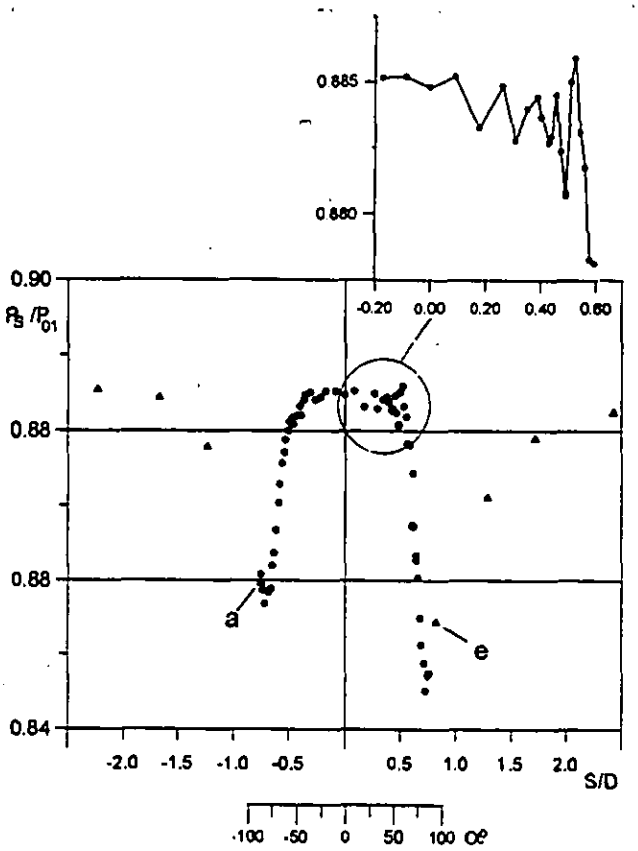

Fig.9: Time averaged base pressure distribution.

4.6 Unsteady trailing edge pressure distribution

Fig.10 shows the root mean square of the fluctuating signal around the trailing edge and upstream of it. The reference system is again the one shown on Fig.3. The points represented by circles stand for the pressure signal acquired with the instrumentation of blade A, while the triangles represent the pressure fluctuations acquired with the instrumentation of blade B. The data scatter is in general of the order of ±0.5% (absolute) with, however, some higher values near the pressure side flow separation point.

The curve presents a small flat region around the centre of the trailing edge with a value of the RMS approximately equal to 4.8% of the downstream dynamic head. The fluctuations increase towards the pressure side and suction side flow separation points. The maximum values and their positions are:

	S/D	α	RMS/Q
S.S	-0.6	68°75	7.8%
P.S	0.775	88°8	8.0%

The two peaks are almost comparable for the values of the RMS, but the abscissa at which they are located are quite different.

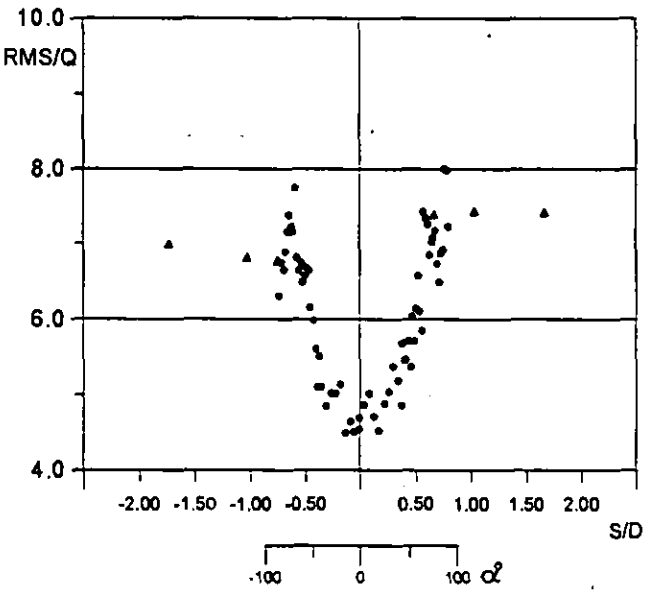

Fig.10: RMS of the fluctuatuing pressure signal around the trailing edge

Moreover one would expect that these locations correspond to the pressure minima in the time averaged pressure distribution, Fig.8. While this is approximately true for the pressure side, on the suction side the peak of the RMS appears to be at a location closer to the centre of the trailing edge. Of course the highest periodic fluctuations are expected to occur at the flow separation points, but this is not necessarily so for the location of the random fluctuations and the RMS values presented bere contain both contributions. It is further interesting to note that these fluctuations are also felt at the same distance upstream of the trailing edge: 7.4% and 6.85% for the pressure side and suction side respectively. The difference may be due to the difference in the boundary layer transition on both sides: natural transition on the suction side and forced transition on the pressure side.

4.7 Time varying pressure oscillations

The periodic character of the pressure oscillation at the trailing edge is clearly shown in Fig.11 which reports the phase averaged

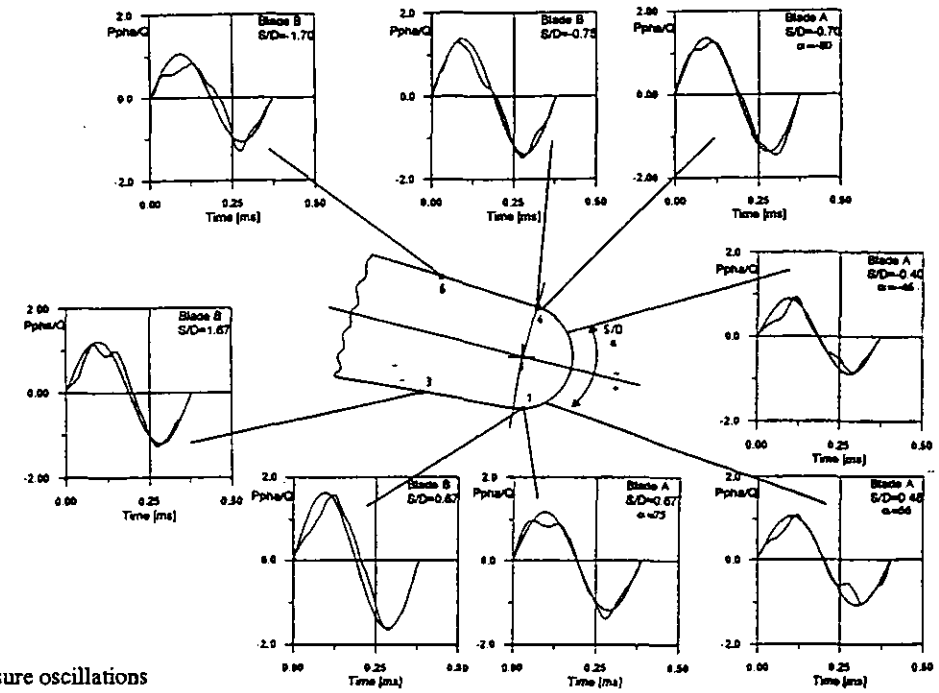

Fig. 11: Time varying pressure oscillations

pressure signals non-dimensionalysed by the downstream dynamic pressure for several locations. Where possible, a comparison between the results coming from blade A and blade B is proposed. The figures show also the comparison with a simple sinusoidal signal having the same period and amplitude as the corresponding experimental signal. The signals have been averaged over 400 cycles. The quality of the phase averaged signals depends on the sharpness of the dominant frequency band of the periodic pressure oscillations. The "best" frequency spectra are those of the transducers positioned near the boundary layer separation points. Each graph indicates the maximum pressure difference over one cycle. Overall the pressure variations appear to be slightly higher on the pressure side. The highest variations occur in the region of the boundary layers separation points. The comparison of the data from blades A and B at these locations is fairly good: on the pressure side 3.28% for blade A and 2.78% for blade B, on the suction side 2.78% for blade A and 2.72% for blade B. Considering that the pressure variations at S/D=±2.5 are still 2.4% and 2.16% for pressure and suction side respectively, it appears that the induced trailing edge vortex pressure variations seem to propagate relatively far upstream. As regards the trailing edge base region, the lack of a dominant vortex shedding frequency did not allow to extract a time varying pressure signal.

5. FLOW VISUALIZATION

5.1 Optical set up

In order to clarify the results coming from the previous tests, it was decided to perform a series of flow visualizations over one vortex shedding cycle. The schlieren technique which was adopted, is a combination of a relatively simple optical arrangement with a high degree of resolution.

The need to avoid blurred images due to the high frequency vortex shedding, requires a specific light source able to provide a very short duration spark. The presented tests were carried out using a Nanolite high speed system manufactured by Impulsphysik, emitting a light spark of 20 nanoseconds duration. The optical arrangement is shown on Fig. 12. The light emitted by the flash lamp is collimated by the lens L and directed toward the test section. The light is then deviated by the flat mirror M1 to the parabolic mirror M2. An image of the source light is formed in the focal point of mirror M2, where a knife edge has been placed. The image is then captured on a Polaroid camera, as shown on Fig. 11.

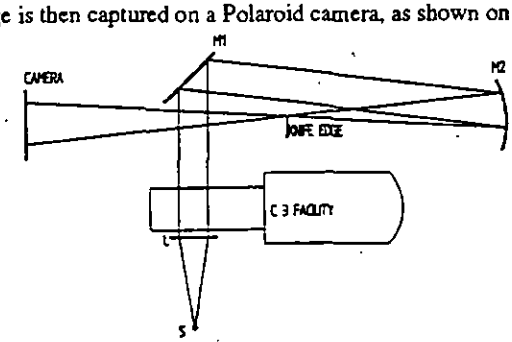

Fig.12: Setup of schlieren system

5.2 Vortex shedding

The schlieren pictures shown in Fig.13 document the formation and the evolution of the vortex street behind the blade trailing edge. The upper blade surface is the blade suction side. Due to the low downstream Mach number, $M_{2is} = 0.4$, the density variations are very weak and hence the vortex patterns in the wake are not as well defined as at high Mach number. Nevertheless, the quality of he flow visualizations is rather satisfactory considering that not only the vortex formation but also the blade surface boundary layers could be clearly visualized. The measurements of the suction side boundary layer thickness from the schlieren photographs of 4-5 mm is in close agreement with the measured boundary layer profile thickness of δ= 4.1 mm in Fig.6. Before discussing the schlieren photographs it may be useful to refer to the description of Gerrard [14] concerning the vortex formation behind cylinders. The model proposed by this author is illustrated in Fig. 14.

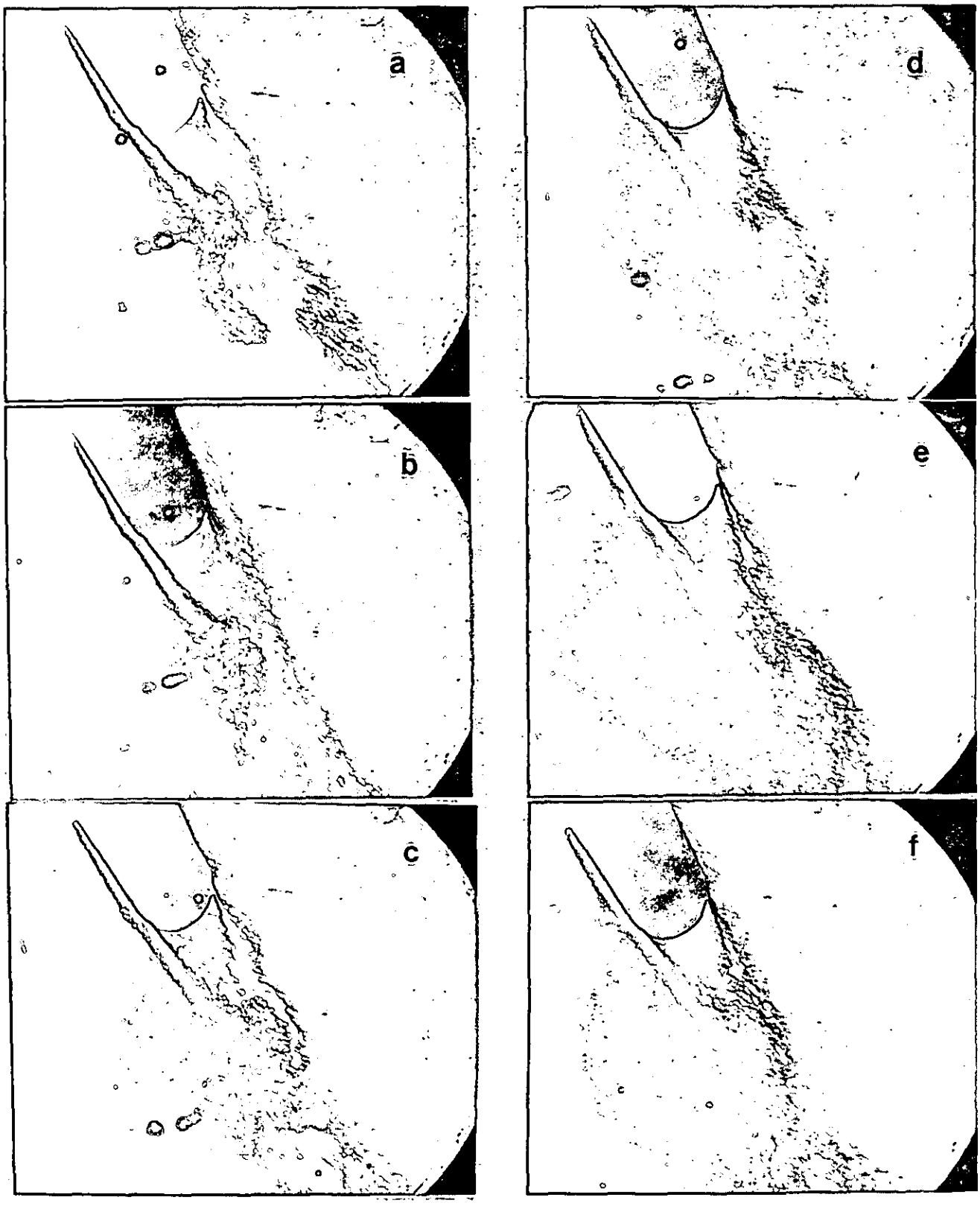

Fig.13a-f: Vortex shedding cycle schlieren pictures

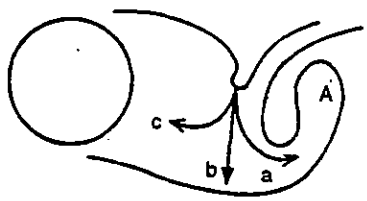

Fig.14: Vortex formation mechanism

The growing vortex (A) is fed by the circulation existing in the upstream shear layer until the vortex is strong enough to entrain fluid from the opposite shear layer bearing vorticity of opposite circulation. When the quantity of entrained fluid is sufficient to cut off the supply of circulation to the growing vortex - the opposite vorticity of the fluid in both shear layers cancel each other - then the vortex is shed off. In picture 13-a, the pressure side vortex is just forming. Its centre appears about 0.8x trailing edge diameter downstream of the blade. The growing vortex approaches the suction side shear layer (13-b) and entrains fluid from it (13-c), as indicated by the curvature of the suction side shear layer to the wake centre. This appears to be also the start of a weak suctinn side vortex. The entrainment of fluid from the opposite shear layer continues until the pressure side vortex is shed off (13-e) and the formation of a new vortex starts. Contrary to the pressure side vortex the evolution of the suction side vortex is much less clear, which suggests a significant difference in the strength of the pressure side and suction side vortices. This result is supported by smoke visualization of Han and Cox [5] behind a turbine guide vane which shows a strong dominance of the pressure side vortex in the wake. The effect of blade circulation appears to be the most appropriate explanation.

Following Gerrard [14] and Berger [15] there is another characteristic parameter which plays a significant role for the vortex shedding: the shear layer thickness referred to by the authors as "diffusion length", which plays a key role in determining the shedding frequency. The thicker the shear layer, the longer it takes for the circulation to be carried across the wake in a sufficient concentration to determine the beginning of the shedding. In the present case the "diffusion length" is quite different for both shear layers and hence the transverse transport of fluid will be different for the formation of the suction side and pressure side vortex. This could possibly lead to an unstahle vortex shedding with as result of a loss in sharpness of the vortex shedding frequency spectrum as observed in the present tests, Fig.8. Finally, the stronger pressure side vortex would explain the higher expansion around the trailing edge as shown in Fig. 9.

6. CONCLUSIONS

The design of a turbine blade with a rotatahle trailing edge cylinder instrumented with a fast responce pressure transducer and a pneumatic wall pressure tapping allowed to measure the steady and unsteady trailing edge pressure distribution with an unusual high spatial resolution. This device allows to determine very accurately the overexpansion at the trailing edge which in the present case exceeded the downstream Mach number by 24% and 19% for the pressure and suction side respectively.

The unsteady pressure measurements showed RMS values for the fluctuating pressure of maximum 8% of the downstream dynamic head near the flow separation points and 4.8% in the base region.

The decomposition of the fluctuating pressure signal into a random and a periodic component showed for the latter a maximum pressure variation of 3% of the dynamic downstream pressure over one cycle.

Both the pressure distribution around the trailing edge and the schlieren photographs of the vortical wake patterns point out the dominance of the pressure side vortex shedding related to the influence of the blade circulation.

AKNOWLEDGMENTS

This research was carried out under contract for the CEC as part of the BRITE EURAM AER2-92-0048 projeci "Time Varying Wake Flow Characteristics behind Flat Plates and Turbine Cascades". The authors wish to acknowledge this support as well as that of MTU and SNECMA.

ANNEXE

Xax	Y	Xax	Y	Xax	Y
0.00	0.00	40.61	21.38	83.83	0.02
0.20	1.75	42.37	21.27	85.07	-1.22
0.75	3.44	44.13	21.10	86.31	-2.48
1.53	5.01	45.87	20.87	87.52	-3.75
2.54	6.47	47.61	20.58	88.72	-5.04
3.67	7.81	49.33	20.23	89.89	-6.35
4.93	9.04	51.05	19.82	91.05	-7.68
6.24	10.22	52.75	19.36	92.19	-9.01
7.60	11.33	54.43	18.85	93.33	-10.36
9.00	12.40	56.10	18.29	94.44	-11.73
10.45	13.40	57.75	17.67	95.54	-13.10
11.93	14.34	59.39	17.00	96.62	-14.49
13.46	15.22	60.99	16.29	97.69	-15.89
15.02	16.03	62.58	15.54	98.75	-17.29
16.62	16.78	64.15	14.73	99.79	-18.71
18.24	17.47	65.70	13.89	100.82	-20.14
19.88	18.11	67.23	13.01	101.83	-21.58
21.54	18.69	68.73	12.10	102.84	-23.03
23.22	19.21	70.21	11.15	103.83	-24.48
24.92	19.68	71.67	10.16	104.81	-25.94
26.63	20.10	73.11	9.14	105.77	-27.41
28.35	20.47	74.52	8.09	106.73	-28.89
30.08	20.77	75.91	7.02	107.67	-30.38
31.83	21.03	77.28	5.91	108.61	-31.87
33.58	21.22	78.63	4.77	109.54	-33.36
35.33	21.34	79.96	3.62	110.46	-34.87
37.09	21.41	81.27	2.45	111.36	-36.37
38.86	21.43	82.56	1.25	112.26	-37.89

113.14	-39.41	149.20	-115.75	181.19	-193.94	39.93	-36.38	99.51	-96.06	147.00	-165.76
114.02	-40.94	149.88	-117.38	181.87	-195.57	41.32	-37.47	100.63	-97.42	147.87	-167.29
114.89	-42.47	150.55	-119.00	182.54	-197.19	42.69	-38.57	101.74	-98.78	148.74	-168.82
115.75	-44.00	151.23	-120.63	183.22	-198.82	44.06	-39.68	102.85	-100.14	149.61	-170.35
116.61	-45.54	151.90	-122.25	183.71	-200.06	45.42	-40.79	103.96	-101.51	150.48	-171.88
117.45	-47.09	152.57	-123.88	183.93	-200.77	46.78	-41.92	105.07	-102.88	151.35	-173.41
118.29	-48.63	153.24	-125.51	184.07	-201.50	48.13	-43.05	106.17	-104.26	152.22	-174.94
119.13	-50.18	153.91	-127.13	184.14	-202.24	49.47	-44.19	107.26	-105.63	153.10	-176.47
119.95	-51.74	154.58	-128.76	184.14	-202.86	50.80	-45.34	108.35	-107.02	153.97	-177.99
120.77	-53.29	155.25	-130.39	184.08	-203.60	52.13	-46.49	109.44	-108.40	154.85	-179.52
121.58	-54.86	155.92	-132.02	183.94	-204.33	53.45	-47.66	110.52	-109.79	155.73	-181.04
122.38	-56.42	156.58	-133.65	183.72	-205.04	54.76	-48.83	111.60	-111.18	156.61	-182.57
123.18	-57.99	157.25	-135.28	183.44	-205.73	56.07	-50.01	112.67	-112.58	157.49	-184.09
123.97	-59.56	157.91	-136.91	183.09	-206.39	57.37	-51.19	113.74	-113.98	158.37	-185.62
124.76	-61.14	158.58	-138.54	182.68	-207.01	58.67	-52.38	114.80	-115.38	159.25	-187.14
125.54	-62.72	159.24	-140.17	182.21	-207.58	59.95	-53.58	115.85	-116.79	160.13	-188.66
126.31	-64.30	159.91	-141.80	181.68	-208.10	61.24	-54.79	116.90	-118.21	161.01	-190.19
127.09	-65.88	160.57	-143.43	0.00	-0.89	62.51	-56.00	117.94	-119.62	161.89	-191.71
127.85	-67.46	161.23	-145.06	0.23	-2.63	63.79	-57.21	118.98	-121.05	162.77	-193.24
128.61	-69.05	161.89	-146.69	0.72	-4.34	65.05	-58.44	120.01	-122.47	163.64	-194.77
129.37	-70.64	162.56	-148.32	1.43	-5.94	66.31	-59.67	121.03	-123.91	164.52	-196.29
130.12	-72.23	163.22	-149.95	2.36	-7.45	67.57	-60.90	122.04	-125.35	165.40	-197.82
130.86	-73.83	163.88	-151.58	3.46	-8.82	68.81	-62.14	123.05	-126.79	166.27	-199.34
131.61	-75.42	164.54	-153.21	4.70	-10.06	70.06	-63.39	124.05	-128.24	167.15	-200.87
132.34	-77.02	165.21	-154.84	6.00	-11.26	71.29	-64.64	125.05	-129.69	168.03	-202.39
133.08	-78.62	165.87	-156.47	7.34	-12.40	72.53	-65.90	126.04	-131.14	168.92	-203.92
133.81	-80.22	166.53	-158.10	8.69	-13.52	73.75	-67.16	127.01	-132.61	169.80	-205.44
134.53	-81.83	167.20	-159.73	10.07	-14.62	74.97	-68.43	127.99	-134.07	170.38	-206.48
135.26	-83.43	167.86	-161.36	11.45	-15.71	76.19	-69.70	128.95	-135.55	170.81	-207.09
135.98	-85.04	168.52	-162.99	12.84	-16.78	77.40	-70.98	129.91	-137.02	171.29	-207.66
136.70	-86.64	169.19	-164.62	14.25	-17.84	78.61	-72.26	130.86	-138.50	171.82	-208.17
137.41	-88.25	169.85	-166.25	15.67	-18.88	79.81	-73.54	131.80	-139.99	172.40	-208.63
138.12	-89.86	170.52	-167.88	17.10	-19.91	81.01	-74.84	132.74	-141.48	173.03	-209.03
138.83	-91.47	171.18	-169.51	18.54	-20.93	82.20	-76.13	133.67	-142.97	173.69	-209.37
139.54	-93.08	171.85	-171.14	19.97	-21.94	83.38	-77.43	134.60	-144.47	174.39	-209.63
140.24	-94.70	172.51	-172.77	21.42	-22.95	84.56	-78.74	135.52	-145.97	175.10	-209.83
140.94	-96.31	173.18	-174.40	22.86	-23.96	85.74	-80.05	136.43	-147.48	175.84	-209.96
141.64	-97.93	173.85	-176.03	24.30	-24.97	86.91	-81.36	137.33	-148.99	176.58	-210.01
142.34	-99.54	174.51	-177.66	25.74	-25.97	88.08	-82.68	138.23	-150.50	177.32	-209.98
143.03	-101.16	175.18	-179.29	27.18	-26.99	89.24	-84.00	139.12	-152.02	178.06	-209.88
143.72	-102.78	175.85	-180.92	28.62	-28.01	90.40	-85.32	140.01	-153.54	178.78	-209.71
144.42	-104.40	176.52	-182.54	30.05	-29.03	91.55	-86.65	140.89	-155.06	179.48	-209.47
145.10	-106.02	177.18	-184.17	31.48	-30.05	92.70	-87.99	141.77	-156.59	180.16	-209.16
145.79	-107.64	177.85	-185.80	32.91	-31.09	93.85	-89.32	142.65	-158.11	180.80	-208.78
146.48	-109.26	178.52	-187.43	34.33	-32.13	94.99	-90.66	143.52	-159.64	181.40	-208.34
147.16	-110.88	179.18	-189.06	35.74	-33.18	96.12	-92.01	144.40	-161.17		
147.84	-112.50	179.85	-190.69	37.15	-34.24	97.26	-93.36	145.26	-162.70		
148.52	-114.13	180.52	-192.32	38.54	-35.30	98.38	-94.71	146.13	-164.23		

The blade coordinates reported here represent only 30% of the entire set. The complete set of coordinates can be downloaded from the FTP site at the von Karman Institute at the following address: **ftp.vki.ac.be/pub/exchange/turbo/asme96/vkiwake.dat**

REFERENCES

[1] CICATELLI, G. and SIEVERDING, C.H.: A Review of the Research on Unsteady Turbine Blade Wake Characteristics. AGARD PEP 85TH Symposium on Loss Mechanisms and Unsteady Flows in Turbomachines. Derby (United Kingdom) 8-12 May, 1995.

[2] LAWACZECK, O.and HEINEMANN, J.: von Karman vortex street in the wake of subsonic and transonic cascades. AGARD Conference Proceedings N. 177 on Unsteady Phenomena in Turbomachinery AGARD CP-177.

[3] SIEVERDING, C.H. and HEINEMANN, H.: The influence on boundary layer state on vortex shedding from flat plates and turbine cascades. J. of Turbomachinery Vol 112 N.2 pp.181-187 April 1990

[4] CARSCALLEN, W.E. and GOSTELOW, J.P.: Observation of vortex shedding in the wake from transonic turbine nozzle vanes. Fifth International Symposium on Transport Phenomena and Dynamics of Rotating Machinery. (ISROMAC-5) Kaanapali, Hawaii, USA May 8-10, 1994

[5] HAN, L.S. and COX, W.R. 1982: A visual study of turbine blade pressure side boundary layer. ASME paper 82-GT-47

[6] MEE, D.J.: Large chord turbine cascade testing at engine Mach and Reynolds number. Exp. in Fluids, Vol136 pp. 321-374, 1983

[7] CANTWELL, B. and COLES, D.: An experimental study of entrainment and transport in the turbulent near wake of a circular cylinder J. of Fluid Mech. Vol. 136 pp 321-374, 1983

[8] HUSSAIN, A.K.M.F. and HAYAKAWA, M.: Eduction of large-scale organized structures in a turbulent plane wake. J. of Fluid Mech. Vol. 180 pp. 193-229, 1983

[9] KIYA, M. and MATSUMURA, M.: Incoherent turbulence structure in the near wake of a normal plate. J. of Fluid Mech. Vol 190 pp 343-356, 1988

[10] LEONARD, O. and VANDENBRAEMBUSSCHE, R.A.: Design method for subsonic and transonic cascade with prescribed Mach number distribution. J. Turbomachinery, Vol.114, N.3, July1992, pp. 553-561

[11] KAWAI, T. and ADACHI, T.: effects of boundary layer fences on secondary flow and losses in a turbine cascade. Int Gas Turbine Congress, Tokyo 1987.

[12] SIEVERDING, C.H.; STANISLAS, M.;SNOECK, J.: The base pressure problem in transonic turbine cascades. J. of Eng for Power, July 1980 Vol. 102.

[13] ZUNINO, P.: Private comunication.

[14] GERRARD, J.H.: The mechanism of the formation region of vortices behind bluff bodies. J. of Fluid Mech. Vol. 25 Part 2 pp.401-413.

[15] BERGER, E.: Jahr. Wis. Ges. L.&R. Berlin.